**SUPPORTING INFORMATION:**

# Axial ligand control over monolayer and bilayer formation of metal-salophens at the liquid-solid interface

**Johannes A. A. W. Elemans,*[a] Sander J. Wezenberg,[b] Michiel J. J. Coenen,[c] Eduardo C. Escudero-Adán,[b] Jordi Benet-Buccholz,[b] Duncan den Boer,[c] Sylvia Speller,[c] Arjan W. Kleij,*[b,d] and Steven De Feyter*[a]**

**Contents:**

# 1. Experimental procedures and analytical data

**General methods and materials:** Zn(3-di-*tert*-butyl-salophen)[1] (**Zn2**) and Zn(5-di-*tert*-butyl-salophen)[2] (**Zn3**) were prepared following previously described procedures. Toluene used for UV-Vis titrations was dried by using a solvent purification system (SPS) from Innovative Technology. All other chemicals were commercial products and were used as received. $^{1}$H NMR and $^{13}$C{$^{1}$H} NMR spectra were recorded on Bruker WM 200 and Avance 400 Ultrashield NMR spectrometers at 297 K. Chemical shifts are reported in ppm relative to tetramethylsilane ($\delta$ = 0.00 ppm) as an internal standard. UV-Vis spectra were acquired on a Shimadzu UV2401PC spectrophotometer. Mass analyses were carried out by the High Resolution Mass Spectrometry Unit at the Institute of Chemical Research of Catalonia (ICIQ), Spain. Elemental analyses were determined by the Elemental Analysis Unit of the University of Santiago de Compostela, Spain.

**Synthesis of metallosalophen complexes**

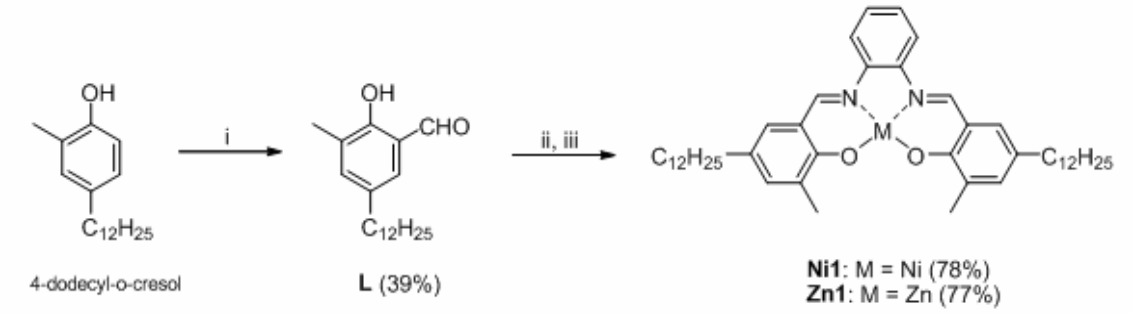


**Scheme S1.** Synthesis of **L** and metallosalophen complexes **Ni1** and **Zn1**: *i*) HMTA, acetic acid, $H_2SO_4$, reflux; *ii*) *o*-phenylenediamine, $Ni(OAc)_2 \cdot 4H_2O$, MeOH; *iii*) *o*-phenylenediamine, $Zn(OAc)_2 \cdot 2H_2O$, MeOH.

**5-dodecyl-2-hydroxy-3-methylbenzaldehyde (L):** 4-dodecyl-*o*-cresol (4.00 g, 14.5 mmol) was combined with hexamethylenetetramine (4.10 g, 29.2 mmol) in 20 mL glacial acetic acid and the mixture was refluxed at 130ºC for 1.5 hr. Then the solution was cooled to 100°C to add 20 mL of an aqueous 33% $H_2SO_4$ solution and the mixture was further refluxed for 1 hr at this temperature. The mixture was transferred to a seperatory funnel whilst hot and the lower water layer was discarded. The remaining red oil was dissolved in 50 mL $Et_2O$ and washed with 25 mL brine and 25 mL $H_2O$, dried over $MgSO_4$ and concentrated. Purification by flash column

[1] A. W. Kleij, M. Kuil, D. M. Tooke, M. Lutz, A. L. Spek, J. N. H. Reek, *Chem Eur. J.*, 2005, **11**, 4743-4750.
[2] E. C. Escudero-Adán, J. Benet-Buchholz, A. W. Kleij, *Inorg. Chem.*, 2007, **46**, 7265-7267.

chromatography (silica gel, eluent 0.5% $Et_2O$ in hexane) yielded an off-white oil, which solidified upon storage at –18ºC (1.74 g, 39%). $^1$H NMR ($CDCl_3$, 400 MHz): δ = 11.09 (s, 1H; O*H*), 9.84 (s, 1H; C*H*O), 7.21 (br, 1H; Ar-*H*), 7.17 (d, *J* = 1.96 Hz, 1H; Ar-*H*), 2.55 (t, *J* = 7.72 Hz, 2H; Ar-C$H_2$), 2.25 (s, 3H; Ar-C$H_3$), 1.58 (m, 2H; C$H_2$), 1.36-1.25 (m, 18H; C$H_2$), 0.88 (t, *J* = 6.84 Hz, 3H; C$H_3$); $^{13}$C{$^1$H} NMR ($CDCl_3$, 100 MHz): δ = 196.9 (*C*=O), 158.2 (*C*-O), 138.6, 133.9, 130.5, 126.7, 119.9 (Ar-*C*), 34.9, 32.1, 31.6, 29.8 (3), 29.7, 29.6, 29.5, 29.3, 22.8 (*C*$H_2$), 15.2, 14.3 (*C*$H_3$) ppm; ESI(+)-MS: m/z = 327.2 $[M+Na]^+$, 249.2 $[M-(CH_2)_3CH_3]^+$; elemental analysis calcd. (%) for $C_{20}H_{32}O_2$: C 78.90, H 10.59; found: C 78.95, H 10.45.

**Ni(3-di-methyl-5-di-dodecylsalophen) (Ni1):** 5-dodecyl-2-hydroxy-3-methylbenzaldehyde **L** (146 mg, 0.48 mmol) and *o*-phenylenediamine (23 mg, 0.21 mmol) were dissolved in 5 mL MeOH. Whilst stirring, $Ni(OAc)_2{\cdot}4H_20$ (60 mg, 0.24 mmol) in 3 mL MeOH was added to the yellow solution and a brown precipitate formed rapidly. The solution was stirred for 16 hr and then the precipitate was filtered off and further washed with hot MeOH and hot acetone. Dried at air to yield a brown solid (122 mg, 78%). $^1$H NMR ($CDCl_3$, 400 MHz): δ = 8.15 (s, 2H; C*H*N), 7.64 (m, 2H; Ar-*H*), 7.20 (m, 2H; Ar-*H*), 7.06 (br, 2H; Ar-*H*), 6.92 (br, 2H; Ar-*H*), 2.48 (t, *J* = 7.66 Hz, 4H; Ar-C$H_2$), 2.29 (s, 6H; Ar-C$H_3$), 1.58 (m, 4H; C$H_2$), 1.36-1.23 (m, 36H; C$H_2$), 0.88 (t, *J* = 6.82 Hz, 6H; C$H_3$); $^{13}$C{$^1$H} NMR ($CDCl_3$, 100 MHz): δ = 164.4 (*C*-O), 153.8 (*C*=N), 143.2, 136.7, 129.8, 129.4, 129.0, 126.9, 118.7, 114.7 (Ar-*C*), 35.0 (Ar-*C*$H_2$), 32.0, 31.4, 29.9, 29.8 (3), 29.7, 29.5 (2), 22.8 (*C*$H_2$), 16.7 (Ar-*C*$H_3$), 14.3 (*C*$H_3$) ppm; Maldi(+)-MS: m/z = 736.5 $[M]^+$; elemental analysis calcd. (%) for $C_{46}H_{66}N_2NiO_2$: C 74.89, H 9.02, N 3.80; found: C 74.34, H 9.15, N 3.73.

**Zn(3-di-methyl-5-di-dodecylsalophen) (Zn1):** 5-dodecyl-2-hydroxy-3-methylbenzaldehyde **L** (113 mg, 0.37 mmol) and *o*-phenylenediamine (18.7 mg, 0.17 mmol) were dissolved in 5 mL MeOH. Whilst stirring, $Zn(OAc)_2{\cdot}2H_20$ (41 mg, 0.19 mmol) in 5 mL MeOH was added and the orange solution was stirred for 16 hr. The orange precipitate was filtered off, washed with MeOH and dried at air (103 mg, 77%). $^1$H NMR ($d_6$-DMSO, 400 MHz): δ = 8.91 (s, 2H; C*H*N), 7.84 (m, 2H; Ar-*H*), 7.33 (m, 2H; Ar-*H*), 7.05 (d, *J* = 3.48 Hz, 4H; Ar-*H*), 2.33 (t, *J* = 7.44 Hz, 4H; Ar-C$H_2$), 2.17 (s, 6H; Ar-C$H_3$), 1.54 (br, 4H; C$H_2$), 1.34-1.18 (m, 36H; C$H_2$), 0.84 (t, *J* = 6.68 Hz, 6H; C$H_3$); $^{13}$C{$^1$H} NMR ($d_6$-DMSO/$d_5$-Py (10:1, v/v), 100 MHz): δ = 169.8 (*C*-O), 162.9 (*C*=N), 139.7, 135.1, 132.2, 130.3, 126.9, 125.5, 117.6, 116.3 (Ar-*C*), 34.2 (Ar-*C*$H_2$), 31.3, 31.1, 29.0 (4), 28.9, 28.7 (2), 22.1 (*C*$H_2$), 17.1 (Ar-*C*$H_3$), 13.8 (*C*$H_3$) ppm; Maldi(+)-MS: m/z = 742.4 $[M]^+$; elemental analysis calcd. (%) for $C_{46}H_{66}N_2O_2Zn{\cdot}H_2O$: C 72.46, H 8.99, N 3.67; found: C 72.44, H 8.87, N 3.91. Crystals of **Zn1-Py** suitable for X-ray diffraction were obtained from a concentrated solution of the Zn-complex in DMSO/pyridine (95:5 v/v)

**STM procedures**

STM images were obtained using a PicoSPM (Agilent) operating in constant current mode with the tip immersed in the solution at room temperature (20–25°C). Pt/Ir (80/20%) tips were used and prepared by mechanical cutting. The graphite lattice was recorded by lowering the bias voltage to –0.05 V immediately after obtaining images of the 2D structures of the organic layers. The drift was corrected using this graphite lattice in Scanning Probe Image Processor (SPIP) software (Image Metrology A/S). All components were first dissolved in 1-phenyloctane before applying a droplet of the solution on a freshly cleaved graphite substrate (HOPG, grade ZYB, Advanced Ceramics Inc., Cleveland, USA).

# 2. Magnifications of STM images, computer-modeled structures of the monolayers, and statistics

## 2a. STM data for Ni1

*Structure of the monolayer*

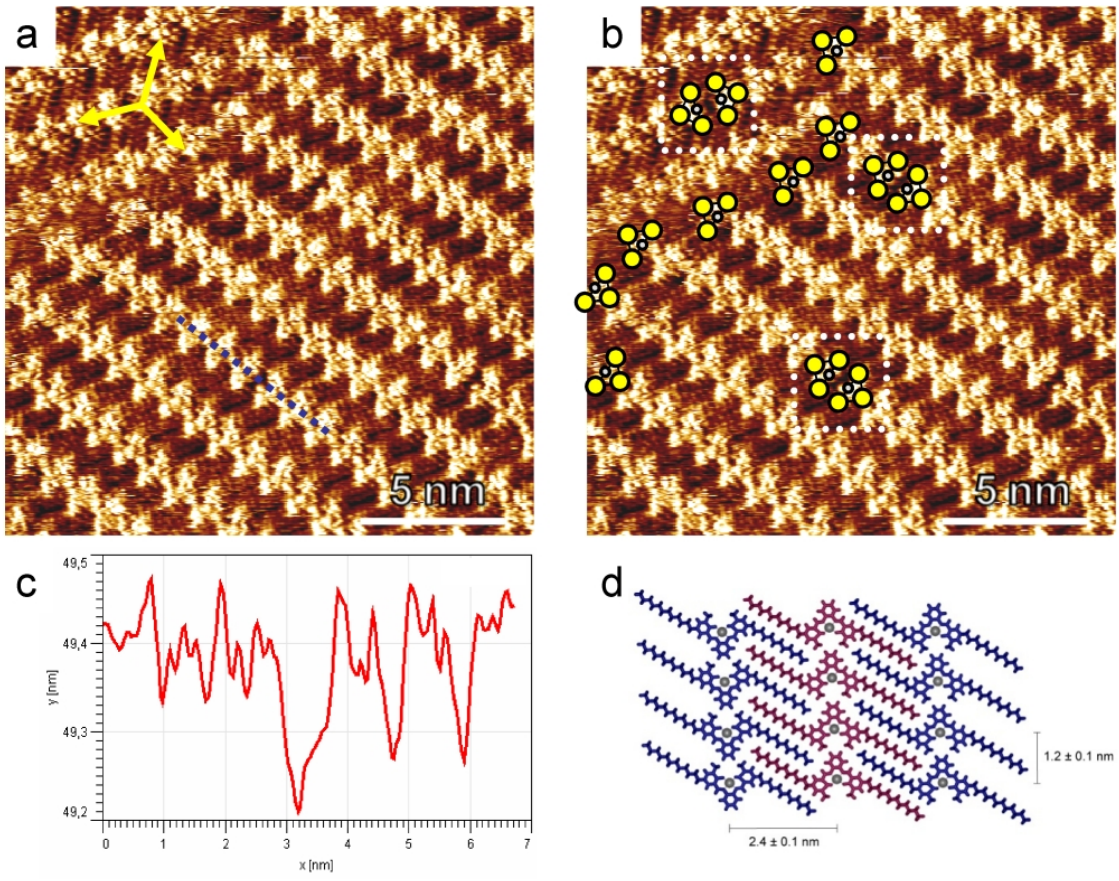


**Fig. S1** (a) Magnified view of the STM image of **Ni1** in Fig. 1a. The yellow arrows indicate the main symmetry directions of the underlying graphite lattice. (b) The same image with schematically highlighted (in yellow) the molecular orientations at domain boundaries and defects; defects are indicated by dashed white squares. (c) Cross section corresponding to the dashed blue trace in Fig. S1(a). (d) Computer-modeled image of parts of three lamellar arrays of **Ni1**, indicating the lamellar periodicity and the distance between the molecules within an array;

*Statistics*

Within the monolayer domains, the head-to-tail arrangement of molecules of **Ni1** in adjacent lamella is either aligned or oppositely directed. By inspecting many monolayer domains, this directionality appeared rather random, but with a slight preference for alignment between adjacent lamellae: statistics on 10 different domains, containing in total 72 lamellae, revealed that 60% of these had an adjacent lamella in which the head-to-tail arrangement was aligned, whereas 40% had an opposite arrangement.

**2b. STM data for Zn1**

*Structures of the molecular layers*

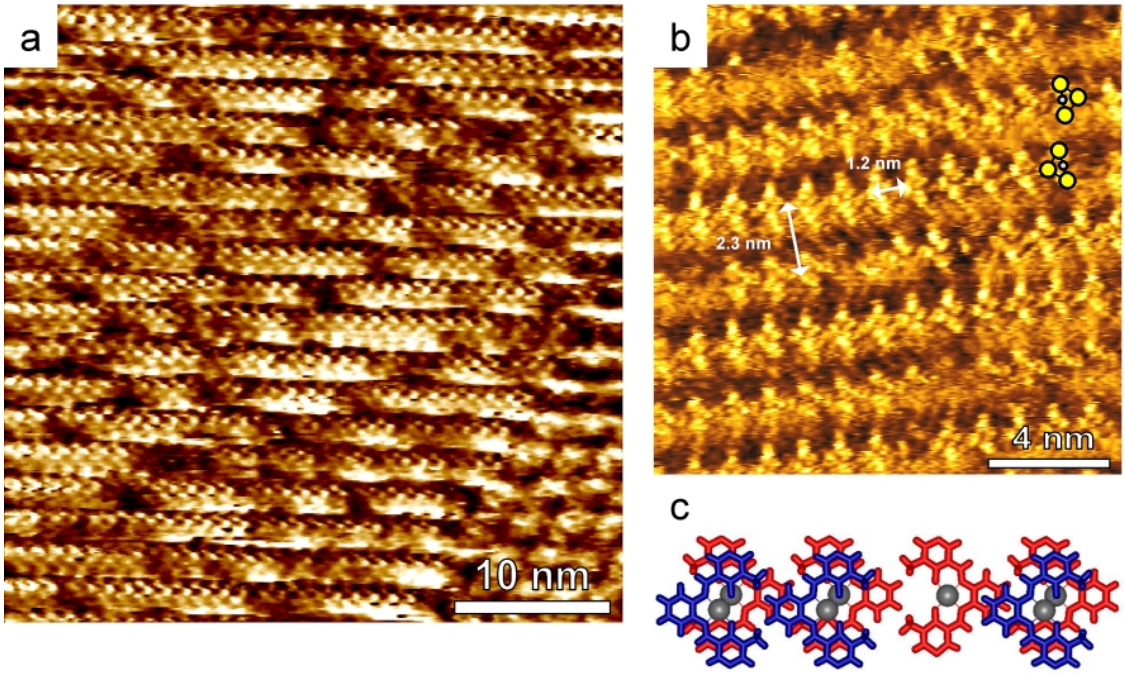


**Fig. S2** (a) Magnified view of the STM image in Fig. 2a (mainly **Zn1** bilayers). (b) Another STM image of mainly bilayer structures of **Zn1**. Repeating distances and two schematic molecules are drawn in. (c) Proposed arrangement of the molecules of **Zn1** within a lamellar array. Three dimers and one monomer are shown. Alkyl chains have been omitted for clarity.

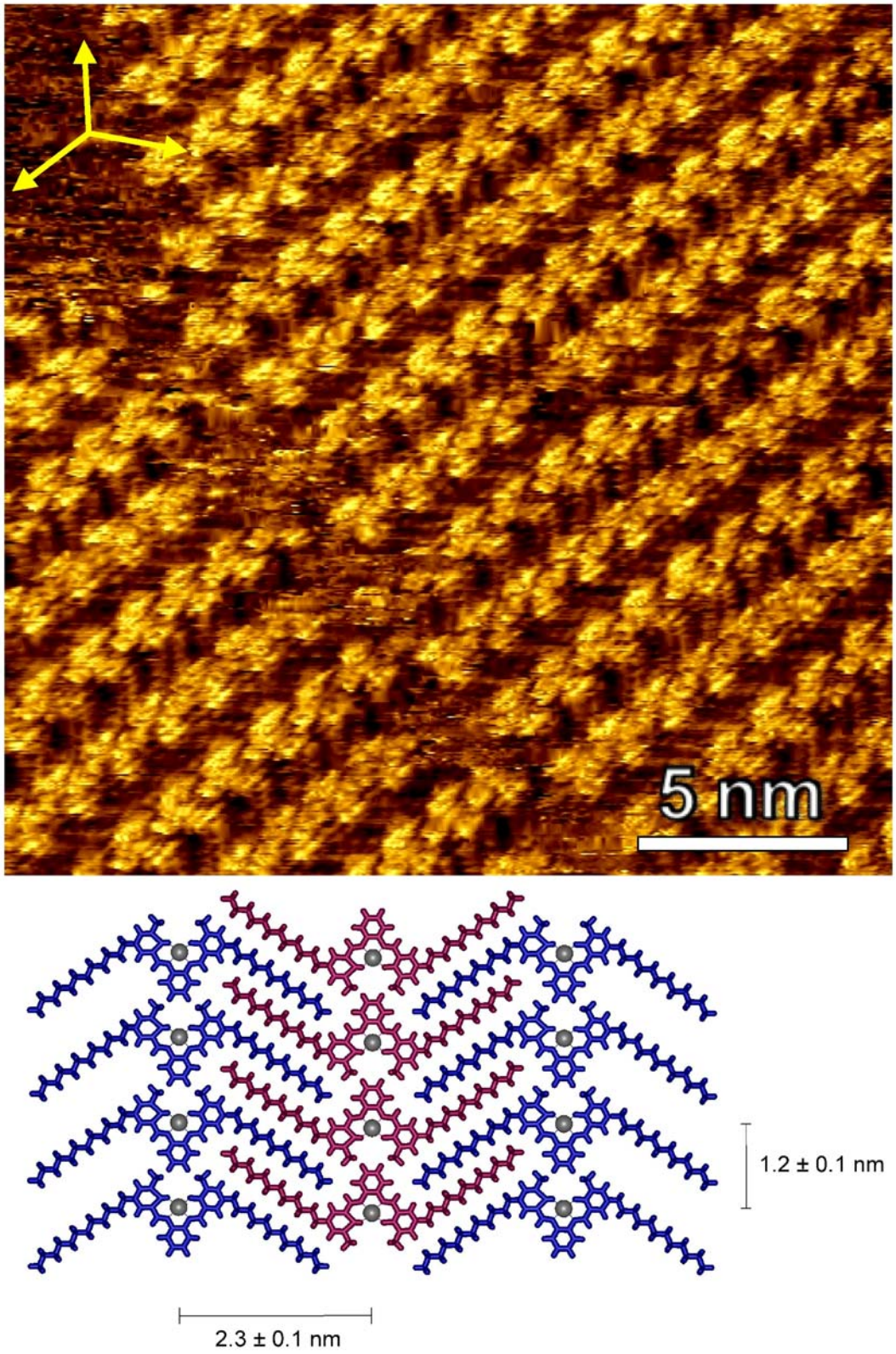


**Fig. S3** Magnified view of the STM image in Fig. 2e (top) and computer-modeled image of parts of three lamellar arrays in a *monolayer* of **Zn1** (bottom), indicating the lamellar periodicity and the distance between the molecules within an array; the yellow arrows indicate the main symmetry directions of the underlying graphite lattice.

*Statistics*

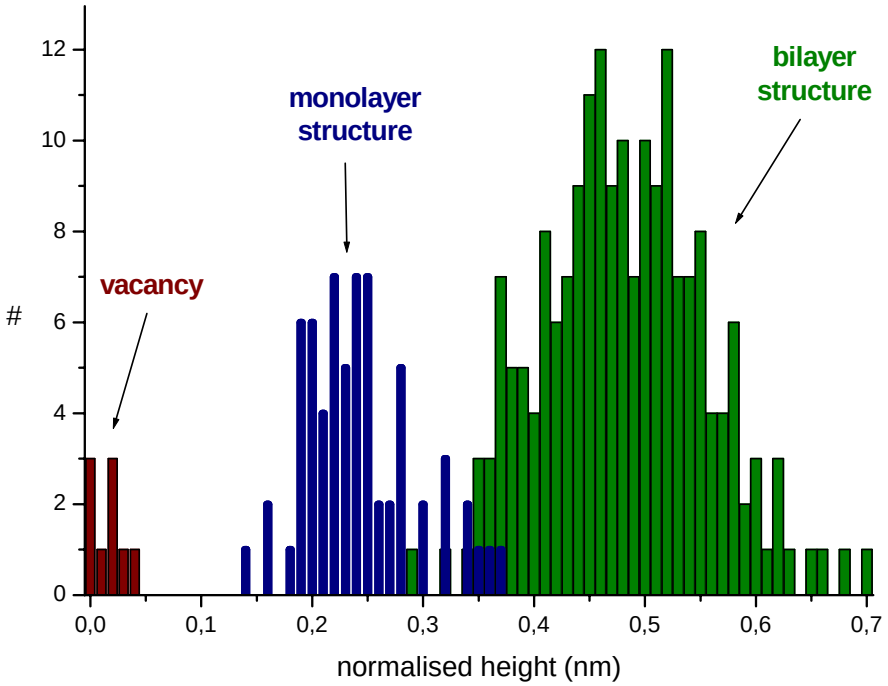


**Fig. S4** Height distribution diagrams of the bilayer-like domains of **Zn1**. Heights of vacancies (blue), single molecules of **Zn1** in a monolayer-like structure (red) and in a bilayer-like structure (green) are depicted. About 20 domains in ten different STM images were used, $n$ = 252. Data are normalised against the lowest observed vacancy height (0.0 nm). The relative abundances of the various species are: vacancy 4%, monolayer structure 29%, bilayer structure 67%.

**2c. STM data for the complex of Zn1 and pyridine**

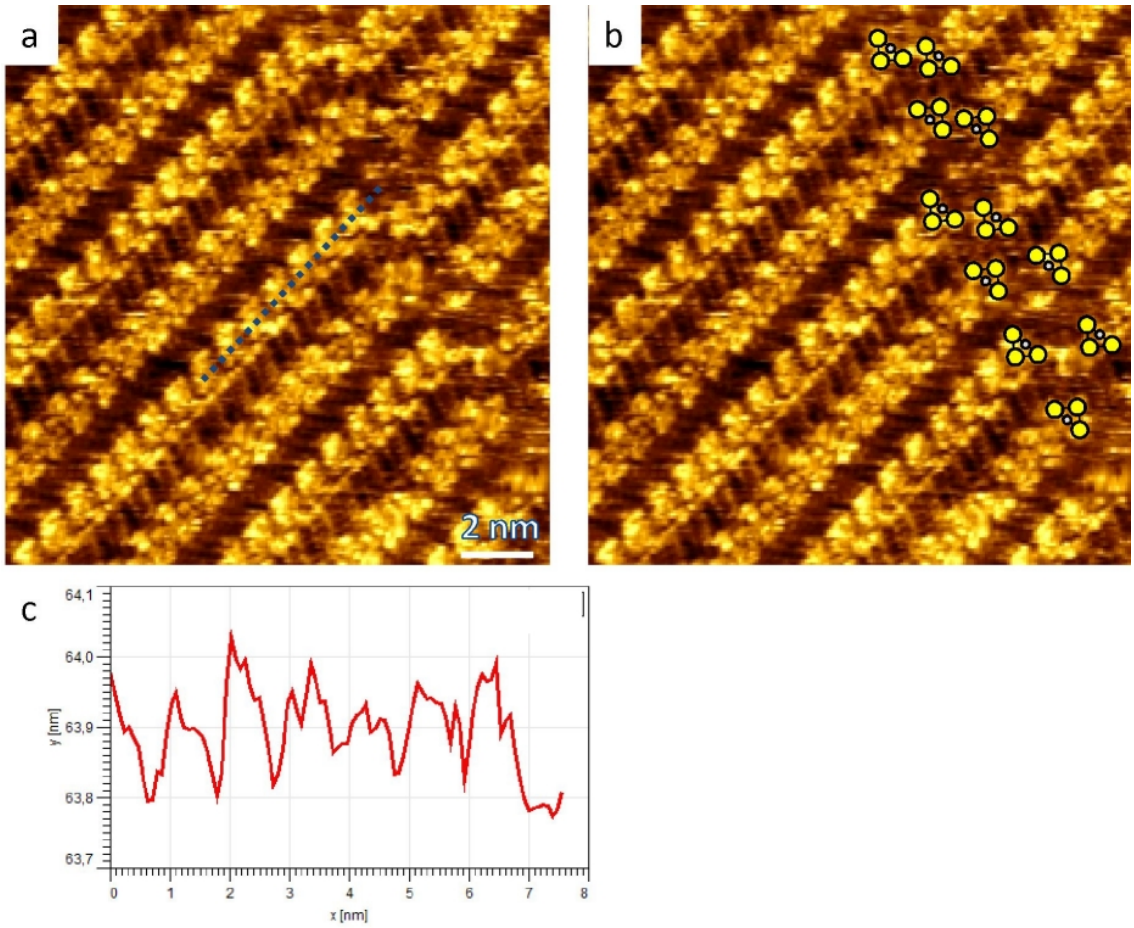


**Fig. S5** (a) Magnified STM image of the complex between **Zn1** and pyridine. (b) The same image with schematic orientations of Zn-salens at the domain boundary drawn in. (c) Cross section corresponding to the dashed blue trace in Fig. S5(a).

## 3. NMR studies

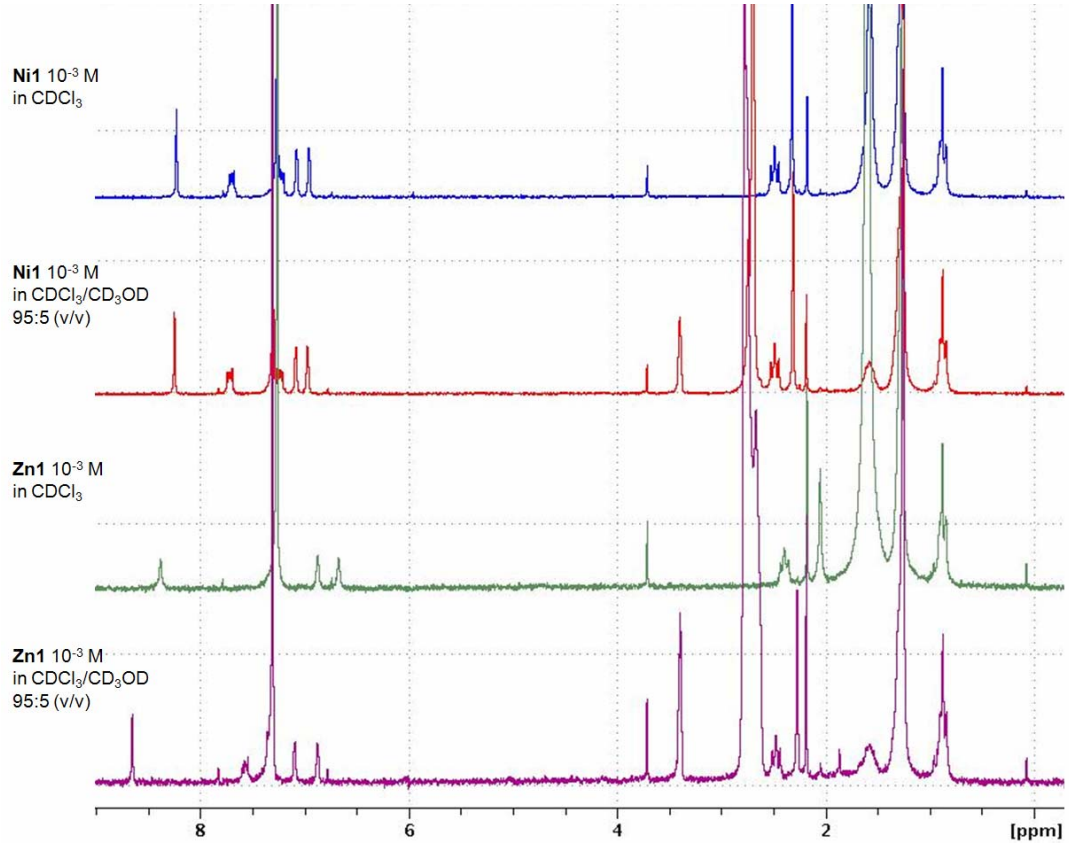


**Fig. S6** $^{1}$H NMR spectra (200 MHz) of **Ni1** and **Zn1** in various solvents.

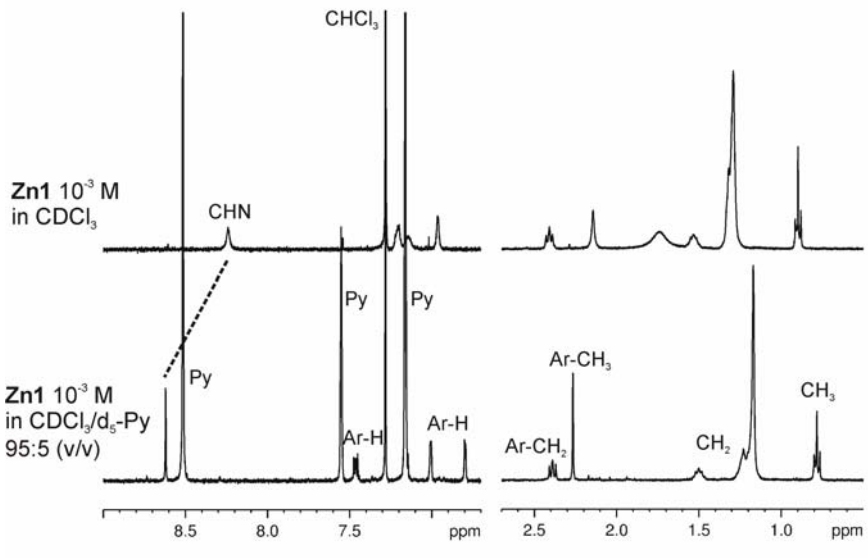


**Figure S7** $^{1}$H NMR Spectra (400 MHz) of **Zn1** in $CDCl_3$ and 5%$d_5$-Py/$CDCl_3$. Signals in the upper spectrum are broadened and assigned to the dimeric Zn(salphen) complex [**Zn1**]$_2$. Pyridine addition leads to sharpened signals and a significant down-field shift for the imine

(CHN) proton, which is in line with the expected break-up of the dimeric structure and formation of a 1:1 **Zn1**-Py complex.

**NMR dillution studies**

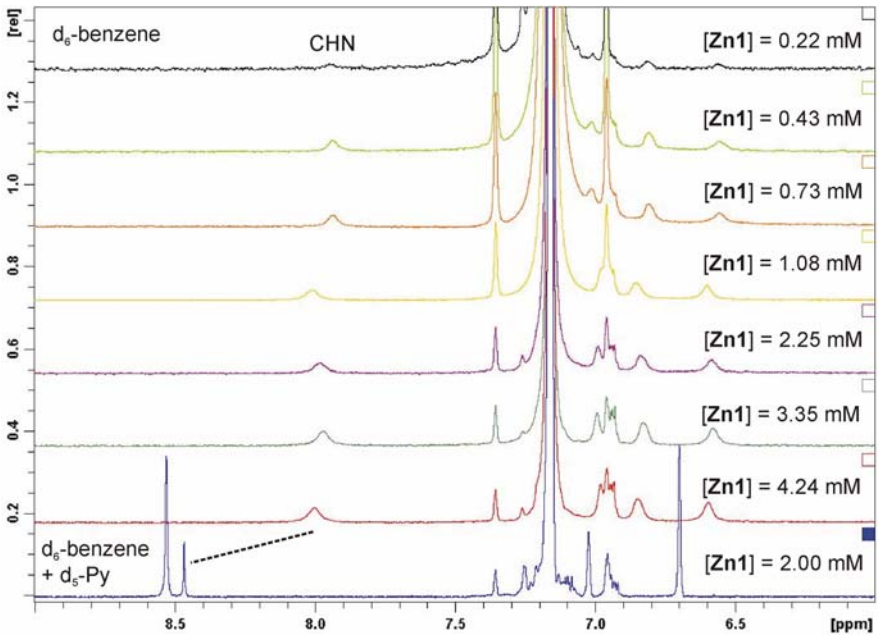


**Figure S8** Aromatic region of the $^{1}$H NMR spectra of **Zn1** at different concentrations in $d_6$-benzene and after addition of $d_5$-pyridine (last spectrum). No significant spectral changes were noted upon dilution in this concentration range. After pyridine addition however, the imine signal was significantly displaced (downfield shift) and all signals became sharper, which points to break-up of the dimeric structure.

# 4. UV-vis titration studies

**Determination of the dimerisation constant using UV-Vis titrations**

Dilution experiments may be used to determine dimerisation constants, but for **Zn1** and related molecules dilution did not provoke significant changes in both UV-Vis absorption and $^1$H NMR spectra. Therefore, the dimerisation constant was determined for **Zn3** by monitoring the disruption of the dimeric complex upon the addition of competitive pyridine (see Scheme S2). It has been established that Zn(salophen) complexes having two *tert*-butyl substituents in the 3-position do not or scarcely form dimers due to the large steric impact, whereas dimeric complexes can be observed for a number of complexes that lack these substituents (for NMR support of this feature refer to Figure S9).[3] As the electronic properties of **Zn2** are highly similar to those of **Zn3**, with the difference that dimerisation is minimal or absent, this compound was used to determine a representative association constant for pyridine binding. Addition of pyridine to **Zn2** resulted in an increase of the absorption maximum at $\lambda$ = 420 nm and successive fitting of the titration data to a 1:1 binding model using *SPECFIT* software[4] gave: $K_{py}$ = 5.89 (± 0.10) x $10^5$ $M^{-1}$ (Fig. S10), which is in good agreement with previously reported association constants for these kinds of complexes.

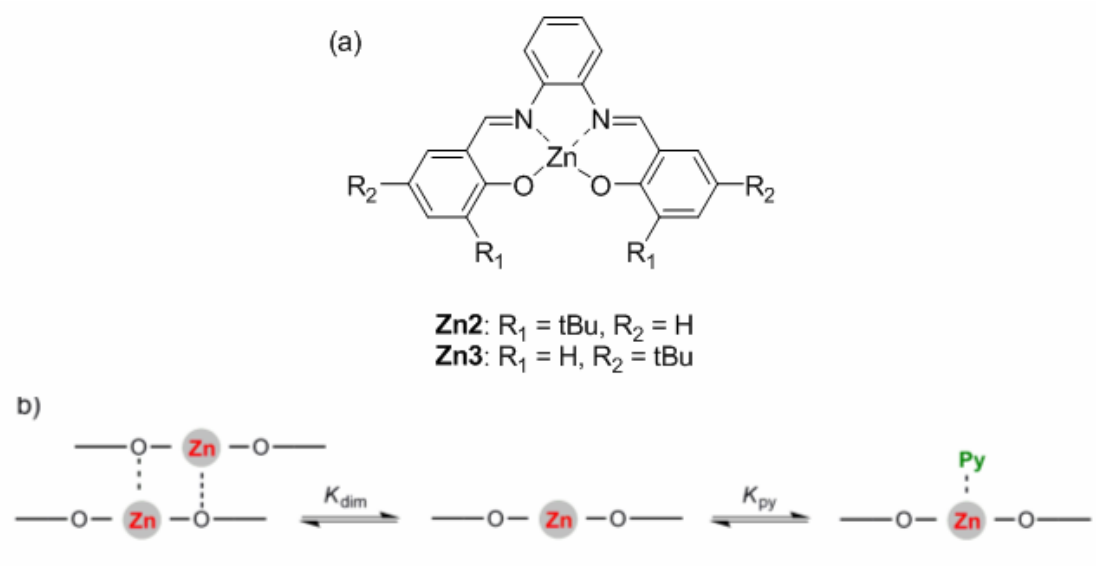


**Scheme S2.** (a) Compound **Zn2** and **Zn3** that were used to determine the dimerisation constant and (b) the involved equilibria. $K_{dim}$ is the stability constant of the dimeric complex and $K_{py}$ denotes the association constant for pyridine binding.

[3] A. W. Kleij, M. Kuil, M. Lutz, D. M. Tooke, A. L. Spek, P. C. J. Kamer, P. W. N. M. van Leeuwen, J. N. H. Reek, *Inorg. Chim. Acta*, 2006, **359**, 1807-1814.
[4] *SPECFIT*/32, version 3.0.40, Spectra Software Associates, R. A. Binstead, A. D. Zuberbühler, 1993-2007; original publication: H. Gampp, M. Maeder, C. J. Meyer, A. D. Zuberbühler, *Talanta*, 1985, **32**, 95-101.

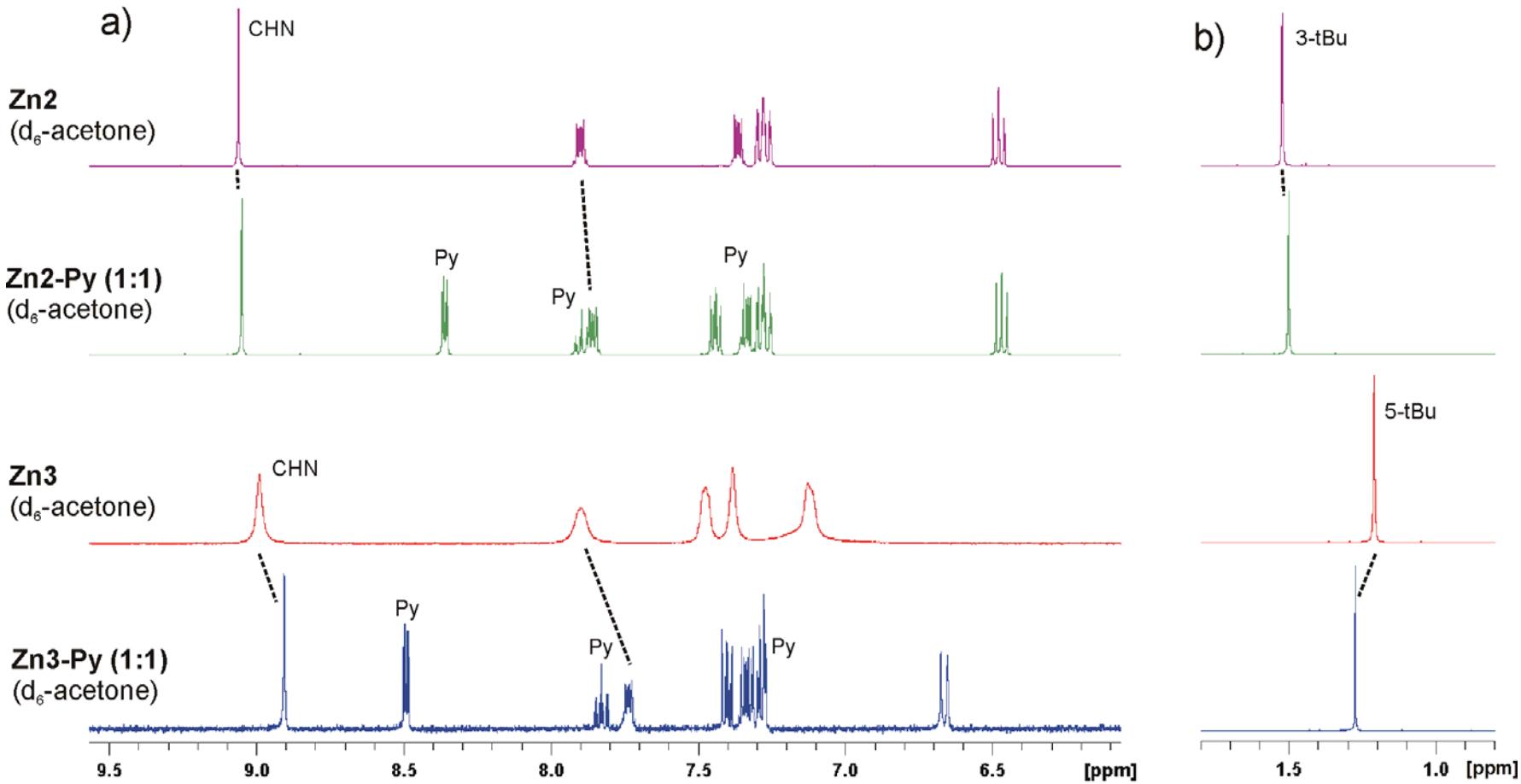


**Figure S9** Aromatic (a) and aliphatic (b) region of **Zn2** and **Zn3** in presence and absence of one equivalent op pyridine. Only **Zn3** shows changes that are indicative of the dissociation of a dimeric species. Please note also the broadened signals for dimeric **Zn3.**

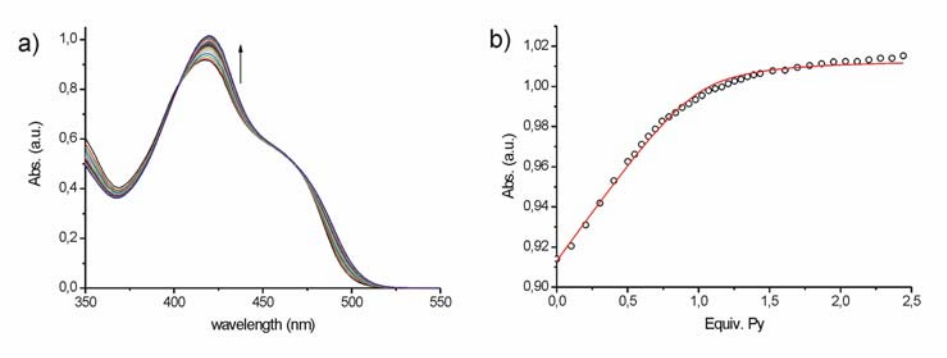


**Figure S10.** (a) Spectral changes of complex **Zn2** upon addition of pyridine carried out in toluene at [Zn] = 4.87 x $10^{-5}$ M and (b) the corresponding titration curve and data fit at 420 nm.

When a similar titration with pyridine was carried out using **Zn3**, very different spectral curves were obtained (Fig. S11). A clear isosbestic point can be observed at λ = 400 nm, illustrating that here more species are involved as compared to the titration with **Zn2**. Note that both the characteristic differences of the UV-vis traces of **Zn2** and **Zn3** in the presence of increasing amounts of pyridine, as well as the fact that in both titrations a significantly different inflection point is observed (for **Zn2**: at a 1:1 ratio, Figure S10; for **Zn3** at around a ratio of 10:1, Figure S11) strongly suggest that both species have a different associated state.

The data was again analyzed with *SPECFIT* by curve-fitting as a two-state equilibrium ($K_{dim}$ and $K_{py}$) and presence of three coloured states (dimer, free complex, 1:1 Zn-Py complex). If we fix the value of pyridine association ($K_{py}$ = 5.89 x $10^5$ $M^{-1}$) and besides assume that the absorption spectrum of free **Zn2** is identical to the spectrum of free **Zn3**,[5] then the dimerisation constant is determined as: $K_{dim}$ = 3.22 (± 0.01) x $10^8$ $M^{-1}$.

[5] *SPECFIT* was not able to simulate the spectrum of the free complex because of spectral overlap and its negligible concentration. For that reason the absorption spectrum of **Zn2** was imported and defined as the spectrum of free **Zn3**. Note that also the acquired spectra for the pyridine coordination complexes of **Zn2** and **Zn3** are highly similar.

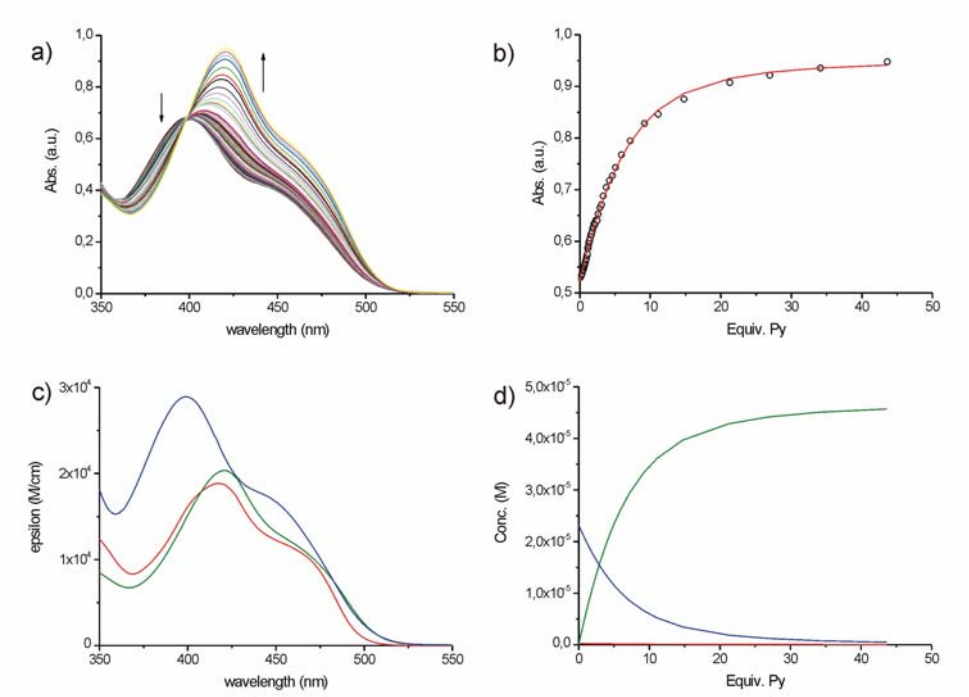


**Figure S11.** (a) Spectral changes of complex **Zn3** upon addition of pyridine carried out in toluene at [Zn] = 4.67 x $10^{-5}$ M and (b) the corresponding titration curve and data fit at 420 nm. (c) Simulated spectra and (d) simulated concentration profiles for the titration at the specified equilibrium constants; blue = dimer, green = Zn-Py complex, red = absorption spectrum of free **Zn2** and concentration profile of free **Zn3**.

**UV-Vis titrations with pyridine.** 5-10 μL aliquots of a pyridine solution in dry toluene ([Py] = 1.00 x $10^{-3}$ M (**Zn2**), 1.01 x $10^{-3}$ and 4.96 x $10^{-3}$ (**Zn3**)) containing the host were added stepwise to 2 mL of a solution of the guest in dry toluene ([Zn] = 4.87 x 10–5 M (**Zn2**), 4.67 x $10^{-5}$ M (**5**)) in a 1 cm quartz cuvet. After each addition a UV-Vis spectrum was acquired.

**UV-vis dillution studies using Zn1**

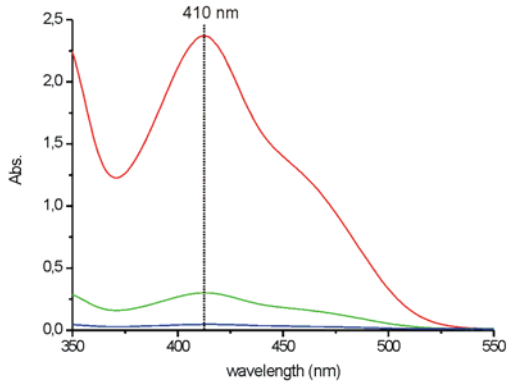


**Figure S12** Absorption spectrum of **Zn1** at $10^{-6}$ (red), $10^{-5}$ (green) and $10^{-4}$ (blue) M. No significant changes in the absorption maximum that are related to break-up of the dimeric structure are noted and thus no dimerisation constant could be determined using this method.

## 5. Displacement ellipsoid plot of the structure of Zn1·Pyr

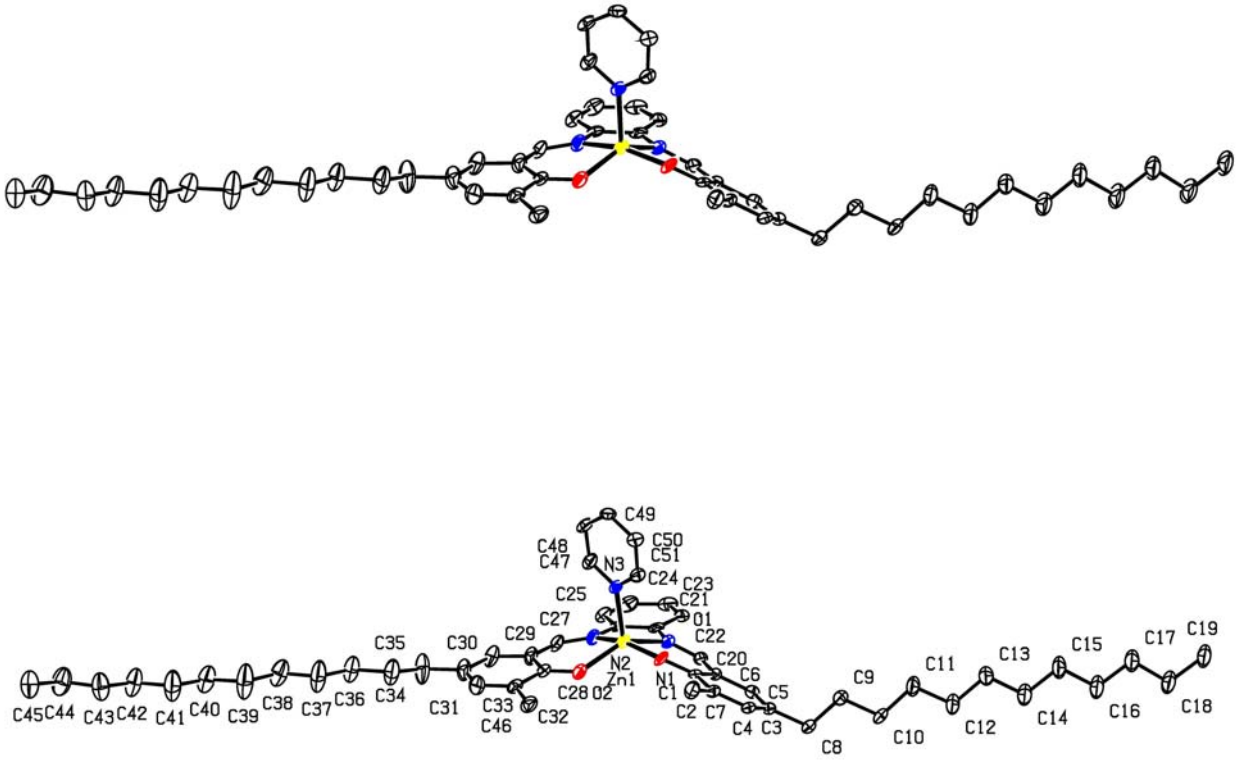


**Figure S13** Ellipsoids are shown at a 50% probability level.